



## Article

# Annealing Effects on SnO<sub>2</sub> Thin Film for H<sub>2</sub> Gas Sensing

Yijun Yang <sup>1,†</sup>, Bohee Maeng <sup>1,†</sup>, Dong Geon Jung <sup>1</sup>, Junyeop Lee <sup>1,2</sup>, Yeongsam Kim <sup>1</sup>, JinBeom Kwon <sup>1</sup>, Hee Kyung An <sup>1</sup> and Daewoong Jung <sup>1,\*</sup>

<sup>1</sup> Advanced Mechatronics R&D Group, Korea Institute of Industrial Technology (KITECH), Daegu 42994, Korea

<sup>2</sup> School of Electronic and Electrical Engineering, College of IT Engineering, Kyungpook National University, 80 Daehakro, Daegu 41566, Korea

\* Correspondence: dwjung@kitech.re.kr; Fax: +82-53-580-0160

† These authors contributed equally to this work.

**Abstract:** Hydrogen (H<sub>2</sub>) is attracting attention as a renewable energy source in various fields. However, H<sub>2</sub> has a potential danger that it can easily cause a backfire or explosion owing to minor external factors. Therefore, H<sub>2</sub> gas monitoring is significant, particularly near the lower explosive limit. Herein, tin dioxide (SnO<sub>2</sub>) thin films were annealed at different times. The as-obtained thin films were used as sensing materials for H<sub>2</sub> gas. Here, the performance of the SnO<sub>2</sub> thin film sensor was studied to understand the effect of annealing and operating temperature conditions of gas sensors to further improve their performance. The gas sensing properties exhibited by the 3-h annealed SnO<sub>2</sub> thin film showed the highest response compared to the unannealed SnO<sub>2</sub> thin film by approximately 1.5 times. The as-deposited SnO<sub>2</sub> thin film showed a high response and fast response time to 5% H<sub>2</sub> gas at 300 °C of 257.34% and 3 s, respectively.

**Keywords:** SnO<sub>2</sub> thin films; metal oxide gas sensor; hydrogen gas sensor; annealing effect

**Citation:** Yang, Y.; Maeng, B.; Jung, D.G.; Lee, J.; Kim, Y.; Kwon, J.; An, H.K.; Jung, D. Annealing Effects on SnO<sub>2</sub> Thin Film for H<sub>2</sub> Gas Sensing. *Nanomaterials* **2022**, *12*, 3227. <https://doi.org/10.3390/nano12183227>

Academic Editor: Michael Tiemann

Received: 29 August 2022

Accepted: 14 September 2022

Published: 16 September 2022

**Publisher's Note:** MDPI stays neutral with regard to jurisdictional claims in published maps and institutional affiliations.



**Copyright:** © 2022 by the authors. Licensee MDPI, Basel, Switzerland. This article is an open access article distributed under the terms and conditions of the Creative Commons Attribution (CC BY) license (<https://creativecommons.org/licenses/by/4.0/>).

## 1. Introduction

Since the industrial revolution, fossil fuels have been used as a major energy source for humanity. However, environmental problems caused by the emission of harmful gases during fuel combustion have emerged, and research on future renewable energy sources, such as solar, nuclear, and wind power, is underway. Among them, hydrogen (H<sub>2</sub>) is attracting attention as a renewable energy source used in various fields, such as automobiles, fuel cells, and chemical industries, because of its environmental friendliness and high energy density characteristics [1,2]. However, H<sub>2</sub> has a flame propagation speed of approximately eight times faster than methane, whereas its minimum ignition energy is approximately 0.06 times lower than methane, which can easily cause a backfire or explosion owing to minor external factors [1,3,4]. To use the H<sub>2</sub> gas in the industry environment, H<sub>2</sub> stability should be ensured, and the detection of gases in the environment containing H<sub>2</sub> is inevitable. H<sub>2</sub> is a colorless, odorless, and volatile gas with a relatively high lower explosive limit of 4%. Therefore, detection by concentration at low and high concentrations and fast response time are significant in H<sub>2</sub> sensing [3].

Based on the method of detection, H<sub>2</sub> gas sensors are generally divided into contact (electrochemical, semiconductor, and solid electrolyte sensor), composite (photoionization and total reflection sensor), and optical type sensors (non-dispersive infrared, and photoacoustic sensor) [1,5]. The semiconductor gas sensor detects the target gas by reading a change in the resistance owing to the difference in the electronic density of a semiconductor surface of the sensing unit when gas flows. This sensing method is advantageous because semiconductor gas sensors are inexpensive, can be easily manufactured in large quantities through microelectromechanical system processes, has a simple configu-

ration of detection circuits, and can detect various types of gases. However, because semiconductor gas sensors are driven at relatively high temperatures, they mainly use a metal-oxide-semiconductor form that is stable at high temperatures. Materials commonly used for metal oxide gas sensors include ZnO [4], SnO<sub>2</sub> [6–8], and TiO<sub>2</sub> [1], among which SnO<sub>2</sub> has been extensively studied as SnO<sub>2</sub> film-structured gas sensors exhibit high response results and fast response rates for specific gases, owing to their unique characteristics. SnO<sub>2</sub> is an n-type semiconductor with a wide energy band gap of 3.6 eV and a tetragonal rutile structure caused by oxygen vacancy. In an n-type semiconductor such as SnO<sub>2</sub>, when external thermal energy is applied, an oxygen vacancy layer acts as a donor to change the number of electrons, thereby adjusting the grain boundary that influences the electrical conductivity and gas sensitivity of the semiconductor film. Therefore, SnO<sub>2</sub> is mainly studied to adjust the electrical conductivity and gas sensitivity by controlling the thickness and grain size of the SnO<sub>2</sub> thin film. In 1971, Naoyshi studied the first gas sensor that used SnO<sub>2</sub> as a sensing material [6]. Thenceforth, various studies have been reported for SnO<sub>2</sub> deposition methods, such as the sol-gel method [6], thermal evaporation [9], radio frequency (RF) sputtering [10], chemical vapor deposition [11], and the ion-beam method [12]. Among them, RF sputtering has been extensively investigated with the commercial advantages of a uniform deposition rate, cost-effectiveness, and high reproducibility. However, high energy deposition can result in unevenness or damage to the film. To improve performance and complement disadvantages of SnO<sub>2</sub> film by sputtering, various post-treatment methods, such as annealing [13,14], acid treatment [15], and plasma treatment [16], were studied. Among them, the annealing method influences the shape and size of the crystal grains of the SnO<sub>2</sub> thin film, changes the oxygen vacancy by the injected O<sub>2</sub> gas in the annealing process, and changes the characteristics of the thin film.

In this study, the SnO<sub>2</sub> thin film was deposited on a glass substrate using RF sputtering and applied as an H<sub>2</sub> gas sensor. Our research aims to develop a high-performance sensor that can detect H<sub>2</sub> more sensitively than general SnO<sub>2</sub> sensors by optimizing the annealing time condition of SnO<sub>2</sub> thin films and exploring the sensor operating temperature. In addition, based on the optimization conditions, it was attempted to maximize the H<sub>2</sub> sensing ability by minimizing the problem of interference with other gases, which most metal oxide-based MOS sensors face.

## 2. Materials and Methods

### 2.1. Sensor Fabrication

The SnO<sub>2</sub> thin film was deposited using RF sputtering. A glass wafer was used as the substrate, and Au was deposited using E-beam evaporation in advance to form an interdigitated electrode. The 99.99% purity target of SnO<sub>2</sub> was used as a sputtering source under a base pressure of  $5 \times 10^{-6}$  torr. Ar and O<sub>2</sub> gases were used as reaction gases under a flow rate of 10 sccm, and deposition energy of 150 W was applied. The SnO<sub>2</sub> thin film, with dimensions of 2.7 × 2.85 mm, was deposited on the glass substrate, with a dimension of 5 × 5 mm. Subsequently, the deposited SnO<sub>2</sub> thin film was annealed at 500 °C under air condition, which was annealed for 1–5 h, with intervals of 2 h. The schematic image of the full fabrication is shown in Figure 1.

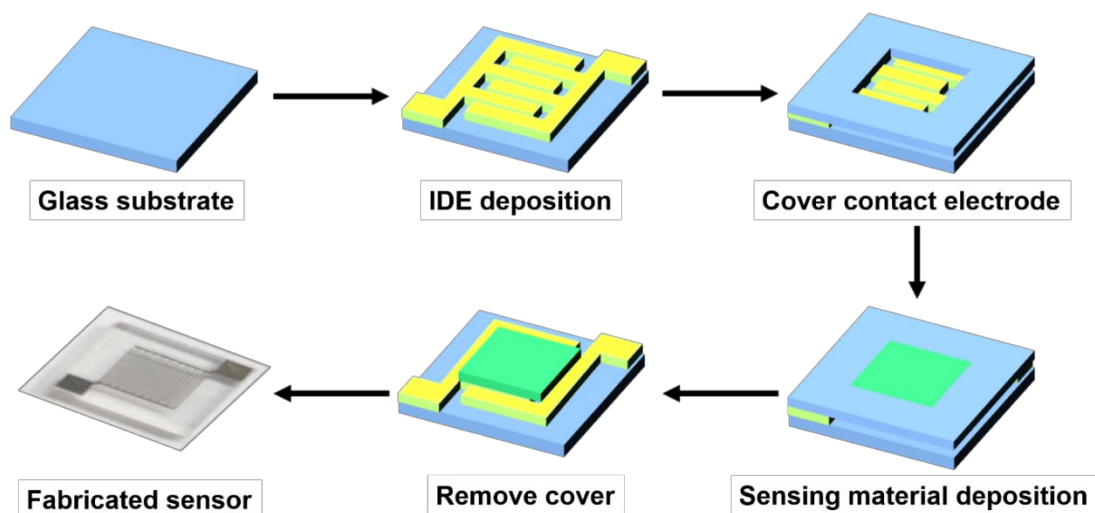


Figure 1. Schematic for SnO<sub>2</sub> gas sensor fabrication.

## 2.2. Sensor Characterization

The X-ray diffraction (XRD, model Empyrean, Panalytical) was used to analyze the crystal structure before and after annealing of the deposited SnO<sub>2</sub> thin film, and a field emission scanning electron microscope (model SU8220, Hitachi) was used for surface morphology and film thickness analysis. The atomic force microscope (AFM, model NX20, Park Systems) was used for surface characterization, and the hydrogen gas sensing performance was evaluated in the manufactured gas chamber, as shown in Figure 2. In the experiment, H<sub>2</sub> gas concentration was adjusted using a mass flow controller (MFC), and a voltage of 1 V was applied to the gas sensor using a source meter (model B2902B, Keysight) to determine the changes in resistance during sensing caused by changes in the H<sub>2</sub>-air environment. The test was performed by fixing the air and H<sub>2</sub> flow rate sum at 400 sccm using an MFC and adjusting the H<sub>2</sub> concentration ratio. The gas detection experiment was performed by placing the sensor on the ceramic heater in the chamber and raising the temperature of the heater from 150 to 300 °C.

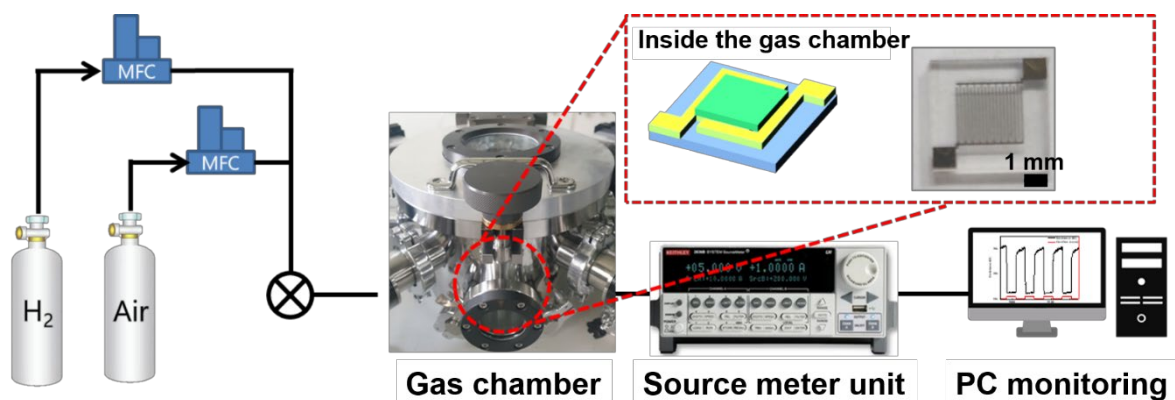


Figure 2. Schematic of gas sensing setup.

## 3. Results and Discussion

### 3.1. Structural and Morphological Characteristics

The crystalline structure is closely related to surface morphology. Based on the annealing process, gas sensing properties are influenced by inducing changes in morphology and structure. In addition, because the sensing process is usually operated at high temperatures, sensors that are annealed after deposition are more stable at the operating temperatures. Metal oxides such as SnO<sub>2</sub> are highly sensitive to annealing, with different

crystalline defects, such as oxygen vacancy or lattice disorder [17]. The grain size of the metal oxide shows a grown pattern under conditions of increasing the annealing time at a fixed temperature or changing the annealing temperature. In our case, the grain morphology change of SnO<sub>2</sub> was confirmed by changing the annealing time under the constant temperature condition of 500°C. The annealing temperature was set through experimental results. SnO<sub>2</sub> thin films were prepared by the RF sputtering method, and these were annealed at a temperature of from 300 to 900°C per 200°C, respectively. The optimal temperature condition was set by measuring the response to the hydrogen of this thin film sensor. The finally set annealing optimum temperature was 500°C. (Figure S3).

XRD patterns show the diffraction peaks of all the samples observed in the SnO<sub>2</sub> pattern (JCPDS no. 41-1445, Figure 3a). From the XRD peaks, the average grain sizes of SnO<sub>2</sub> thin films for different annealing times were calculated using the Scherrer equation:

$$D = \frac{K\lambda}{\beta \cos \theta} \quad (1)$$

where D is the grain size; K is a constant that depends on the crystalline shape and indices with a value of approximately 0.9;  $\lambda$  is the radiation wavelength;  $\beta$  is the crystalline size, measured at half of the maximum intensity;  $\theta$  is the Bragg angle at which peaks are observed [18]. From the Scherrer equation, the average grain size of a SnO<sub>2</sub> thin film was calculated and is denoted in Figure 3b.

As shown in Figure 3b, an increase in annealing time increased SnO<sub>2</sub> grain size. Increases in annealing time result in corresponding increases in grain size. This is because smaller grains are combined into larger grains through high-temperature melting. The annealing time results in a rapid decrease in a non-bridging oxygen defects concentration, thereby forming SnO<sub>2</sub> grains [19]. Therefore, an increase in annealing time can be a factor in increasing grain size [20–22].

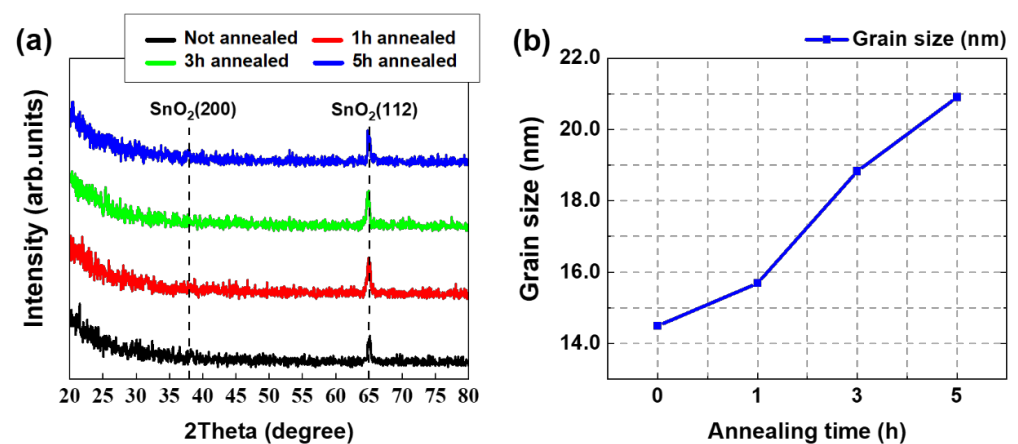


**Figure 3.** (a) XRD of SnO<sub>2</sub> for annealing time; (b) average grain sizes of the SnO<sub>2</sub> thin film with annealing times.

The surface morphologies of SnO<sub>2</sub> thin films from the as-deposited to 5-h annealed thin films, according to annealing time, are shown by the AFM images. As shown in Figure 4, the surface roughness decreased after the annealing time exceeded 1 h. The decrease was more severe when the annealing time exceeded 3 h. The thickness of film which is not annealed SnO<sub>2</sub> was about 55.6 nm by SEM cross-section image (Figure S1). The surface roughness of the as-deposited SnO<sub>2</sub> thin film was 1.042 nm. After annealing for 1 h, the surface roughness slightly increased to 1.066 nm. However, the surface roughness decreased as the annealing time increased, which was 0.921 nm after annealing the deposited SnO<sub>2</sub> for 3 h. The surface roughness further decreased to 0.399 nm after annealing for 5 h, showing a certain difference compared to the others. After annealing for 1 h, the surface

roughness increased because grains grew in the z-direction to the substrate surface, which occurred preferentially. Notably, island coalescence was absent for 1 h. However, after 1 to 5 h, the vertical surface roughness decreased with an increase in grain size, which became lateral. After being subjected to annealing for 1 h, the surface protrusions melted and grew on the lateral side, meaning the grain size increased. This decrease in surface roughness when the annealing time exceeded 1 h resulted from the island coalescence that created a smaller vertical distance to the top of the island [23].

The gas sensor based on an n-type metal-oxide-semiconductor, such as SnO<sub>2</sub>, is significantly influenced by the grain size. As the electrons flow against the energy barriers formed at the grain boundaries, the number of energy barriers decreases as the grain grows. When a SnO<sub>2</sub> film deposited by sputtering was annealed, the SnO<sub>2</sub> grain crumpled. Thus, the surface of the dense film became porous, increasing the reactive area for H<sub>2</sub> gas that is accompanied by increased sensitivity of the SnO<sub>2</sub> film. After annealing, the grain size of SnO<sub>2</sub> increased, and the energy barriers and grain boundary defects decreased [24].

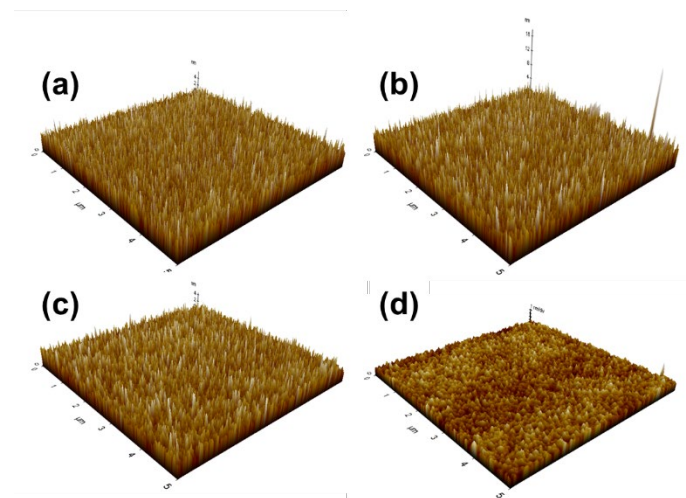


**Figure 4.** AFM surface image of SnO<sub>2</sub> thin film by annealing time; (a) as-deposited not annealed; (b) 1 h. annealed (c) 3-h annealed (d) 5-h annealed

### 3.2. Sensing Performance

We validated the effect of SnO<sub>2</sub> thin films on H<sub>2</sub> by adjusting the annealing time and confirmed the optimal conditions in which the sensor will perform under various operating temperatures.

An experiment to evaluate the SnO<sub>2</sub> sensing performance of H<sub>2</sub> gas was conducted inside the gas chamber by adjusting the internal temperature and gas concentration. The sum of the total flow rates of H<sub>2</sub> gas and air was fixed at 400 sccm, and the concentration of H<sub>2</sub> gas was controlled using the MFC. In the experiment, the sensor response for H<sub>2</sub> gas was calculated as follows:

$$\text{Response, } S(\%) = \frac{\Delta R}{R} \times 100 = \frac{R_0 - R}{R} \times 100, \quad (2)$$

R<sub>0</sub> is the resistance of the sensor measured in the air atmosphere before the H<sub>2</sub> gas injection, and R is the resistance of the sensor exposed to H<sub>2</sub> gas. Because SnO<sub>2</sub> is an n-type semiconductor, the resistance at the time of reaction with the H<sub>2</sub> gas is reduced. Therefore, the response of SnO<sub>2</sub> for H<sub>2</sub> gas is calculated as the difference in the resistance before the reaction to the change in the resistance after exposure to H<sub>2</sub>.

The sensitivity and response time of the 3 h and unannealed SnO<sub>2</sub> for H<sub>2</sub> gas as conducted in the gas chamber of a fixed internal temperature of 300 °C is shown in Figure 5. According to Figure 5a, the response of both 3-h and unannealed SnO<sub>2</sub> increased with an increase in H<sub>2</sub> concentration; however, the response of the 3-h annealed SnO<sub>2</sub> showed a higher value than the unannealed SnO<sub>2</sub> for the same hydrogen concentration. The gap

between the values of the response of the two conditions increased as the difference in H<sub>2</sub> concentration increased. When the H<sub>2</sub> concentration reached 50,000 ppm, the highest response value was observed in the annealed condition (~378%), which was approximately 1.5 times higher than that of the unannealed (~251%). The H<sub>2</sub> sensing response and recovery time of a 3-h annealed SnO<sub>2</sub> as air and hydrogen flow is shown in Figure 5b. The response and recovery time of the 3-h annealed SnO<sub>2</sub> were approximately 12 and 53 s, respectively, under H<sub>2</sub> gas of 50,000 ppm at a chamber of 300 °C. (The graph of the response and recovery time of the sensor without annealing can be confirmed in the supplementary data, Figure S2). Kang *et al.* verified that the initial resistance of SnO<sub>2</sub> increases at some point as the annealing temperature increases [25]. In here, we also confirmed that the resistance value increased from the initial annealing value of 35 K to 80 M during the performed annealing time of 1 to 5 hours (Figure S2). The response time was calculated as the elapsed time for the resistance difference between R<sub>0</sub> and R to decrease from 90 to 10% after H<sub>2</sub> gas injection. Similarly, the recovery time was calculated as the time elapsed for the resistance difference to change from 10 to 90%.

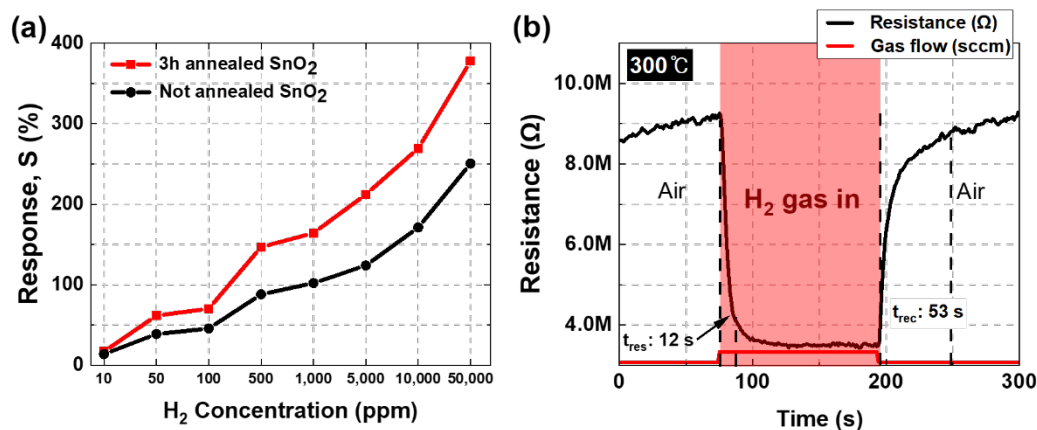


**Figure 5.** (a) Sensitivity of 3-h annealed SnO<sub>2</sub> and not annealed SnO<sub>2</sub> by H<sub>2</sub> concentration; (b) hydrogen response and recovery time of 3-h annealed SnO<sub>2</sub>.

The sensitivity of metal oxides is influenced by many factors, such as the grain size of the material, surface area distribution, and charge carrier on the sensing surface. As shown in Figure 5, the sensitivity gradually increased with the annealing time, and the highest sensitivity was obtained at the 3-h condition. The response time showed a similar tendency to the sensitivity, and the highest value was obtained in the 3-h condition.

The sensitivity is closely related to the surface area and adsorption regions of the sensing gas. With an increase in grain size, the sensitivity of SnO<sub>2</sub> also increases with the surface area. Therefore, the 3-h annealed SnO<sub>2</sub> had a larger surface area and a larger grain size than the unannealed and 1-h-annealed SnO<sub>2</sub> films. This increased the sensitivity (according to the previous measurements, the grain size of SnO<sub>2</sub> increased with the annealing time (Section 3.1)). Figure 6 describes the charge transfer situation when the grain size is increased by performing annealing. In general, the electrical conductivity of semiconducting thin films is increased with annealing because, during the annealing treatment, it is influenced by the tunneling of the charge carriers through the barriers of the grain boundary and the recrystallization of grains [22,26]. The grain size is one of the significant factors that control resistance. The size of the crystallites is determined by directly manipulating the active surfaces (spread-out) of the thin films [22]. An increase in the diameter of the crystallites decreases the spread-out surface of the layer that is formed by the nanocrystallites' decrease. The effect of annealing increases the extended (active) surface at a certain cleavage limit of the resulting crystal, and thus the resistance value decreases [22,27].

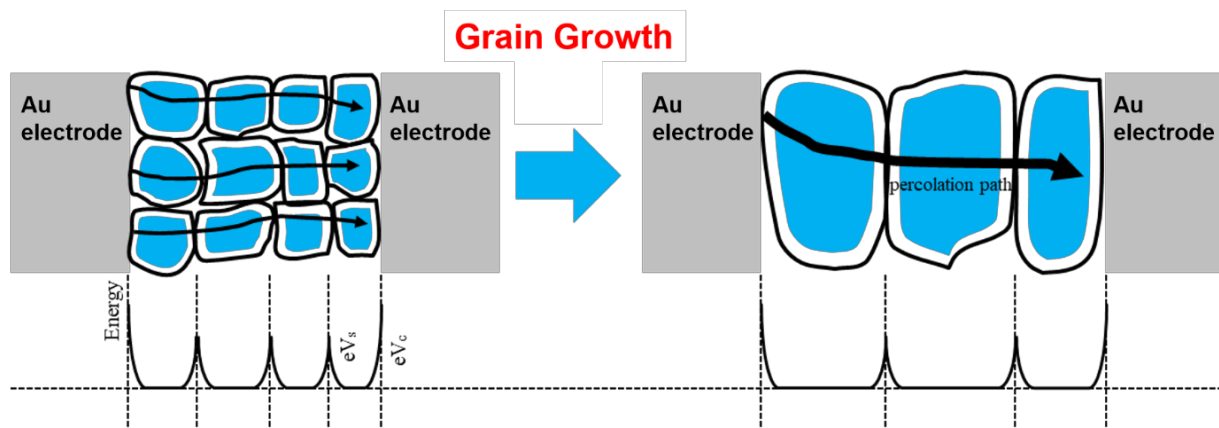


**Figure 6.** Schematic image of SnO<sub>2</sub> grain boundary and Schottky barrier with Au electrode before and after annealing.

The response and recovery times were also expected to increase with the increasing grain size of SnO<sub>2</sub> because a longer time is required to respond to more adsorption/desorption of H<sub>2</sub> gas on the surface of the sensing materials. Moreover, a larger time is required for saturation and recovery to the initial values, as shown in Figure 7. Lee *et al.* validated that the heat treatment was essential to induce changes in the gas sensing film morphology that was more stable to be operated at the sensing temperature, and the response time increased when annealing was applied [19].

However, according to Figure 7, the response of the 5-h annealed SnO<sub>2</sub> showed the lowest sensitivity, although the grain size increased. This lowered reactivity is considered to be a phenomenon caused by surface roughness, as shown in Figure 4. The total surface area of SnO<sub>2</sub> annealed for 5 h was reduced compared to others, and the sensitivity to H<sub>2</sub> was also reduced.

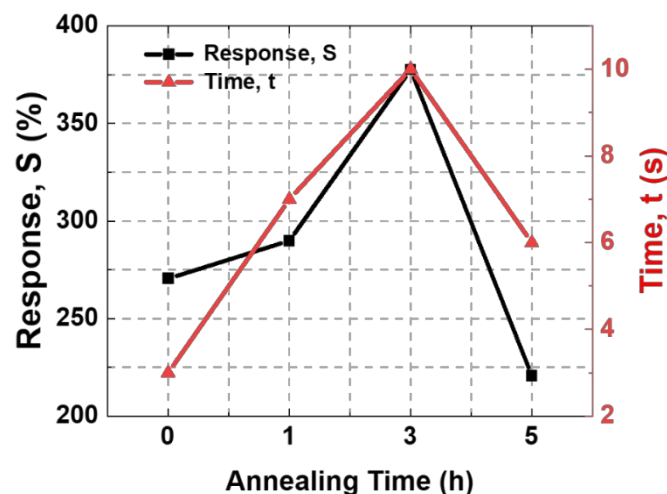


**Figure 7.** Sensitivity and response time for annealing time of SnO<sub>2</sub> thin film under a 300 °C gas reaction condition.

Metal oxide-based gas sensors have different performance values according to changes in the operating temperature, owing to their sensing principle. Moreover, the response time is highly influenced by the operating temperature. As shown in Figure 8a, the sensitivities of all the sensors, i.e., the 1, 3, and 5-h-annealed sensors, increased up to the operating temperature of 300 °C. Furthermore, the response time of the 3-h-annealed SnO<sub>2</sub> decreased as the temperature increased, as shown in Figure 8b. Although the sensitivity and response time improved with an increase in operating temperature, the sensing tool

was adversely influenced by the high operating temperature of the gas chamber. Therefore, the experiment was limited to temperatures of at most 300 °C.

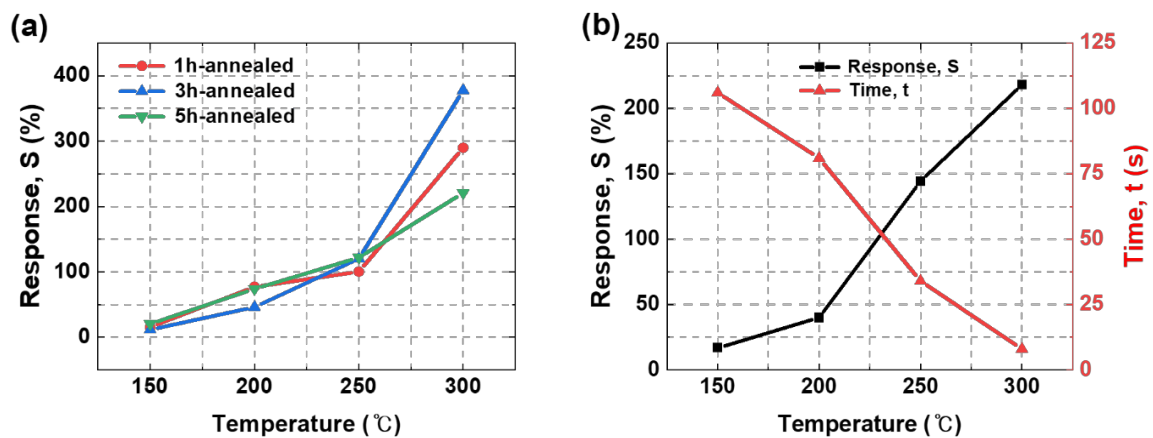


**Figure 8.** (a) Comparison of response according to the operating temperature of sensors fabricated under different annealing conditions. (b) Comparison of sensitivity and response time according to sensor operating temperature of H<sub>2</sub> sensor fabricated by annealing for 3 h.

Furthermore, we believe that the different optimal working temperatures for the sensors can be explained by assuming that two electron barriers exist between the SnO<sub>2</sub> grains and Au electrodes [28]. One is the barrier between individual SnO<sub>2</sub> grains, and the other is between the SnO<sub>2</sub> and Au electrodes. A charge transfer by gas adsorption/desorption must traverse the two barriers to the measuring device (multimeter). Thus, as the temperature increases, the kinetic energy of the electrons increases, and more electrons can easily jump over the two barriers and move faster than at a lower temperature. Therefore, sensitivity and response time can be improved, as shown in Figure 8.

The selectivity of the SnO<sub>2</sub> thin film to other gases was also validated. In addition to H<sub>2</sub>, CO<sub>2</sub>, NH<sub>3</sub>, and NO<sub>2</sub> were reacted with the SnO<sub>2</sub> thin sensor at 300 °C. The gas sensing mechanism of the metal oxide-based hydrogen detection sensor consists of a chemical reaction between chemically absorbed oxygen and the target gas. The selectivity results for each gas of the SnO<sub>2</sub> thin film are shown in Figure 9. The response to CO<sub>2</sub> with the same concentration of 50 ppm as H<sub>2</sub> was the lowest at 3.89%. In the case of NO<sub>2</sub> and NH<sub>3</sub> gas, the sensor reacted with a low gas concentration of 50 and 20 ppm, respectively, owing to the risk of toxicity. The responses with these gases were 10.99% and 13.76%, respectively. Our gas sensor shows a high response to hydrogen. It is because our hydrogen sensor sets the optimal conditions for the high response, therefore exhibiting excellent reactivity compared to other gases. Another reason is that resistance deviation and the optimized temperature vary depending on the type of sensing gas. For example, NH<sub>3</sub> shows the highest response for SnO<sub>2</sub> thin film at about 100–150 °C. This temperature is much lower than the sensor operating temperature we set for the hydrogen detecting. This selectivity trend has shown that the optimized SnO<sub>2</sub> sensor indicates a better response to hydrogen than NO<sub>2</sub> and NH<sub>3</sub> [28].

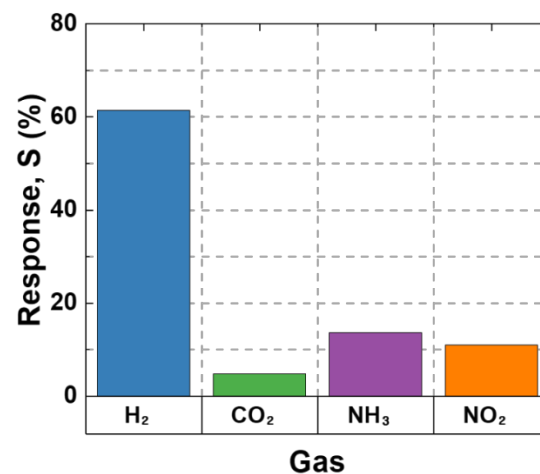


Figure 9. Gas selectivity of SnO<sub>2</sub> thin film.

In sensor applications, results should be consistent for repeated gas reactions to establish the reliability of the measurement values and product commercialization. Repeatability tests for H<sub>2</sub> gas were performed on a SnO<sub>2</sub> thin film sensor annealed for 3 h. The result is shown in Figure 10. The tests were performed at a reaction temperature of 300 °C for 5% H<sub>2</sub> gas, and a consistent gas response was shown without significant damage to the sensor, even after repeated reactions. A stable and reversible reaction was observed, even in the course of the repeated experiments. Based on these results, the SnO<sub>2</sub> thin film sensor fabricated with the RF sputtering method and treated to an optimal annealing process was stable and suitable for use as a H<sub>2</sub> detection sensor.

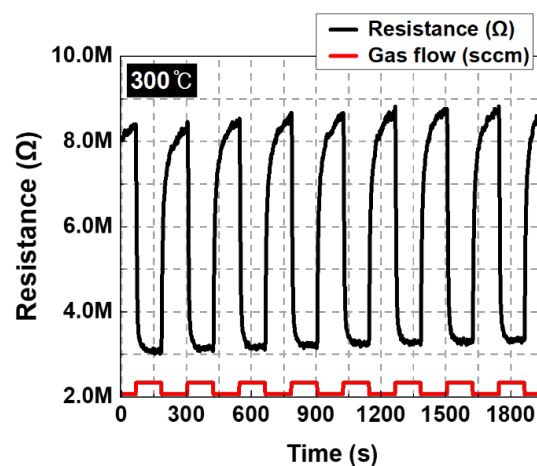


Figure 10. Repeatability tests of 3-h-annealed SnO<sub>2</sub> thin film (5%).

### 3.3. Sensing Mechanism

Gas sensing of SnO<sub>2</sub> functions on the difference in resistance resulting from the properties of n-type semiconductors caused by free electrons inside. The conductivity of the semiconductor gas sensor is controlled by subsequent reactions, such as chemical adsorption, oxidation, and diffusion of oxygen on the tin oxide's surface. This change occurs by gaining electrons from the reaction between absorbed oxygen and H<sub>2</sub> [24].

If free electrons are activated by applying thermal energy to SnO<sub>2</sub>, they are captured on the surface by atmospheric oxygen, as shown in Figure 11a. By capturing the free electrons, the electron depletion layer is formed on the SnO<sub>2</sub> surface, thereby increasing the potential barrier and the internal resistance, as shown in Figure 11b. The chemical equations that explain the capturing of free electrons by oxygen are as follows:



Subsequently, H<sub>2</sub> gas is injected, free electrons react with captured oxygen to form water vapor, the oxygen adsorbed to the surface is removed, the captured free electrons are released, as shown in Figure 11c, potential barriers are lowered, and the internal resistance is reduced. A H<sub>2</sub> sensing reaction is expressed as follows:

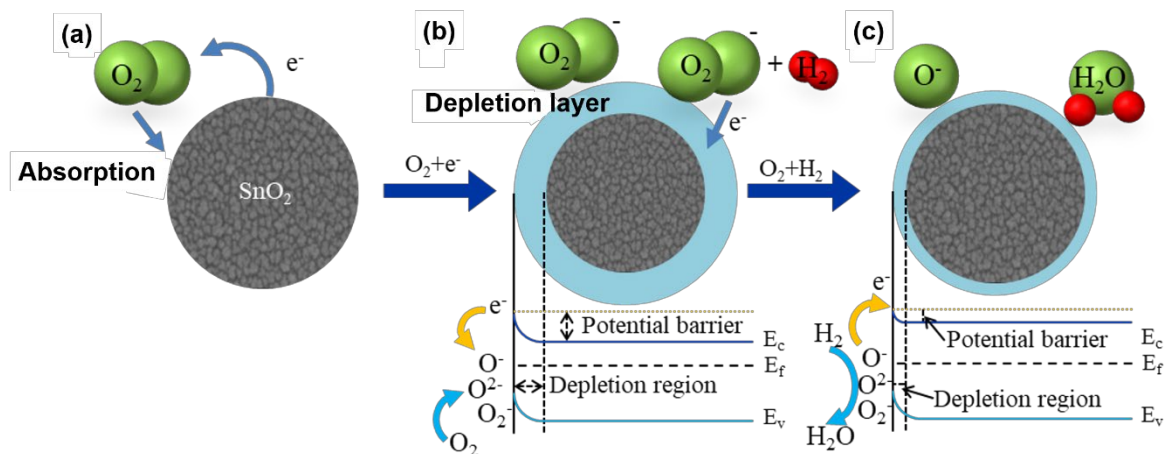
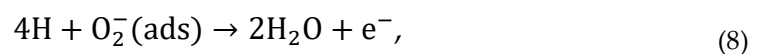
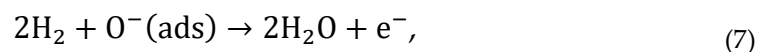
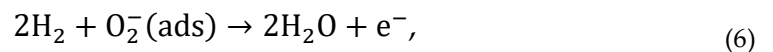


**Figure 11.** n-type metal oxide hydrogen sensing mechanism; (a) SnO<sub>2</sub> as-deposited; (b) SnO<sub>2</sub> in air; (c) SnO<sub>2</sub> in H<sub>2</sub> reduction gas.

#### 4. Conclusions

This study fabricated a SnO<sub>2</sub> thin film gas sensor by depositing a metal oxide-based layer using the RF sputtering technique and annealing under high-temperature conditions. Here, the hydrogen gas detection performance of this SnO<sub>2</sub> thin film sensor, according to the annealing time and gas reaction operating temperature, was demonstrated.

We experimentally validated the H<sub>2</sub> sensing capability of the SnO<sub>2</sub> thin film sensor to improve performance by increasing the metal oxide grain size as the annealing treatment time increased (up to 3 h), which led to the improvement of the surface area for the gas response. In addition, we validated that the improvement of the operating temperature of the gas reaction of the sensor can improve sensor performance and shorten the response time by assisting the electrons to move through the electronic barrier. Our sensor showed excellent selectivity in hydrogen gas compared to other gases. In addition, the sensor could operate without being damaged, even for repeated gas reactions.

This study demonstrated that a robust and stable metal oxide sensor could be manufactured by completing the optimal annealing treatment on the metal oxide thin film introduced by the RF sputtering technique.

**Supplementary Materials:** The following supporting information can be downloaded at: <https://www.mdpi.com/article/10.3390/nano12183227/s1>, Figure S1: Cross-section SEM image of unannealed SnO<sub>2</sub>, Figure S2: Hydrogen response and recovery time of (a) unannealed SnO<sub>2</sub>, (b) 1-h-annealed SnO<sub>2</sub>, (c) 3-h-annealed SnO<sub>2</sub>, and (d) 5-h-annealed SnO<sub>2</sub>, Figure S3: Hydrogen response and time for the annealing temperature.

**Author Contributions:** Conceptualization, D.J. and H.K.A.; methodology, Y.Y., B.M., D.G.J., and J.L.; software, J.L., J.K., and Y.K.; formal analysis, Y.Y. and B.M.; investigation, Y.Y., B.M., and D.J.; writing—original draft preparation, Y.Y. and B.M.; writing—review and editing, Y.Y., B.M., and D.J.; visualization, Y.Y. and B.M.; supervision, B.M. and D.J.; All authors have read and agreed to the published version of the manuscript.

**Funding:** This research received no external funding.

**Data Availability Statement:** Not applicable.

**Acknowledgments:** This study has been conducted with the support of the Korea Institute of Industrial Technology as “Development of holonic manufacturing system for future industrial environment (Kitech EO-22-0001).” This research was financially supported by the Institute of Civil Military Technology Cooperation funded by the Defense Acquisition Program Administration and Ministry of Trade, Industry and Energy of the Korean government under grant No. 21-SF-BR-05. This work was supported by the Korea Innovation Foundation (INNOPOLIS), a grant funded by the Korean government (MSIT) (2020-DD-UP-0348).

**Conflicts of Interest:** The authors declare no conflict of interest.

## References

1. Han, S.D. Review and new trends of hydrogen gas sensor technologies. *J. Korean Sens. Soc.* **2010**, *19*, 67–86.
2. Kadhim, I.H.; Hassan, H.A.; Abdullah, Q.N. Hydrogen gas sensor based on nanocrystalline SnO<sub>2</sub> thin film grown on bare Si substrates. *Nano-Micro Lett.* **2016**, *8*, 20–28.
3. Kim, Y.S. Optimization of Metal Oxide thin Film Thickness and Annealing Conditions for Fabricating High-Sensitivity Hydrogen Sensors for Hydrogen Leakage Detection. Master’s Thesis, Kyungpook National University, Daegu, Korea, 2021.
4. Kang, W. Enhanced hydrogen gas sensing properties of ZnO nanowires gas sensor by heat treatment under oxygen atmosphere. *J. Korean Inst. Surf. Eng.* **2017**, *50*, 125–130.
5. Nazemi, H.; Joseph, A.; Park, J.; Emadi, A. Advanced micro- and nano-gas sensor technology: A review. *Sensors*. **2019**, *19*, 1285–1307.
6. Kadhim, I.H.; Hassan, H.A.; Ibrahim, F.T. Hydrogen gas sensing based on nanocrystalline SnO<sub>2</sub> thin films operating at low temperatures. *Int. J. Hydrog. Energy*. **2020**, *45*, 25599–25607.
7. Chen, Y.; Wang, X.; Shi, C.; Li, L.; Qin, H.; Hu, J. Sensing mechanism of SnO<sub>2</sub>(1 1 0) surface to H<sub>2</sub>: Density functional theory calculations. *Sens. Actuators B Chem.* **2015**, *220*, 279–287.
8. Shanmugasundaram, A.; Basak, P.; Satyanarayana, L.S.; Manorama, V. Hierarchical SnO/SnO<sub>2</sub> nanocomposites: Formation of in situ p–n junctions and enhanced H<sub>2</sub> sensing. *Sens. Actuators B Chem.* **2013**, *185*, 265–273.
9. Sun, S.H.; Meng, G.W.; Zhang, G.X.; Gao, T.; Geng, B.Y.; Zhang, L.D.; Zou, J. Raman scattering study of rutile SnO<sub>2</sub> nanobelts synthesized by thermal evaporation of Sn powders. *Chem. Phys. Lett.* **2003**, *376*, 103–107.
10. Leng, D.; Wu, L.; Jiang, H.; Zhao, Y.; Zhang, J.; Li, W.; Feng, L. Preparation and Properties of SnO<sub>2</sub> Film Deposited by Magnetron Sputtering. *Int. J. Photoenergy*. **2012**, *2012*, 1–6.
11. Liu, Y.; Koep, E.; Liu, M. A Highly sensitive and fast-responding SnO<sub>2</sub> sensor fabricated by combustion chemical vapor deposition. *Chem. Mater.* **2005**, *17*, 3997–4000.
12. Min, B.K.; Choi, S.D. SnO<sub>2</sub> thin film gas sensor fabricated by ion beam deposition. *Sens. Actuators B Chem.* **2004**, *98*, 239–246.
13. Khan, A.F.; Mehmood, M.; Rana, A.M.; Bhatti, M.T. Effect of annealing on electrical resistivity of rf-magnetron sputtered nanostructured SnO<sub>2</sub> thin films. *Appl. Surf. Sci.* **2009**, *255*, 8562–8565.
14. Mehraj, S.; Ansari, M.S.; Alimuddin. Annealed SnO<sub>2</sub> thin films: Structural, electrical and their magnetic properties. *Thin Solid Film* **2015**, *589*, 57–65.
15. Ozaki, Y.; Suzuki, S.; Morimitsu, M.; Matsunaga, M. Enhanced long-term stability of SnO<sub>2</sub>-based CO gas sensors modified by sulfuric acid treatment. *Sens. Actuators B Chem.* **2000**, *62*, 220–225.
16. Hu, K.; Wang, F.; Liu, H.; Li, Y.; Zeng, W. Enhanced hydrogen gas sensing properties of Pd-doped SnO<sub>2</sub> nanofibres by Ar plasma treatment. *Ceram. Int.* **2000**, *46*, 1609–1614.
17. Al-Jumaili, B.E.; Rzaiz, J.M.; Ibraheam, A.S. Nanoparticles of CuO thin films for room temperature NO<sub>2</sub> gas detection: Annealing time effect. *Mater. Today Proc.* **2021**, *42*, 2603–2608.
18. Hu, Y.; Tan, O.K.; Pan, J.S.; Huang, H.; Cao, W. The effects of annealing temperature on the sensing properties of low temperature nano-sized SrTiO<sub>3</sub> oxygen gas sensor. *Sens. Actuators B Chem.* **2005**, *108*, 244–249.
19. Lee, Y.L.; Tsai, W.C.; Chang, C.H.; Yang, Y.M. Effects of heat annealing on the film characteristics and gas sensing properties of substituted and un-substituted copper phthalocyanine films. *Appl. Surf. Sci.* **2001**, *172*, 191–199.

20. Li, P.; Wang, B.; Wang, Y. Ultrafast CO sensor based on flame-annealed porous CeO<sub>2</sub> nanosheets for environmental. *Appl. J. Inorg. Mater.* **2021**, *36*, 1223–1230.
21. Doubi, Y.; Hartiti, B.; Hicham, L.; Fadili, S.; Batan, A.; Tahri, M.; Belfhaili, A.; Thevnin, P. Effect of annealing time on structural and optical proprieties of TiO<sub>2</sub> thin films elaborated by spray pyrolysis technique for future gas sensor application. *Mater. Today* **2020**, *30*, 823–827.
22. Ahmeda, N.M.; Sabaha, F.A.; Abdulgafour, H.I.; Alsadig, A.; Suliemane, A.; Alkhoaryeff, M. The effect of post annealing temperature on grain size of indium-tin-oxide for optical and electrical properties improvement. *Results Physics* **2019**, *13*, 102159.
23. Simões, A.Z.; González, A.H.M.; Zaghete, M.A.; Varela, J.A.; Stojanovic, B.D. Effects of annealing on the crystallization and roughness of PLZT thin films. *Thin Solid Films* **2001**, *384*, 132–137.
24. Barsan, N.; Koziej, D.; Weimar, U. Metal oxide-based gas sensor research: How to? *Sens. Actuators B Chem.* **2007**, *121*, 18–35.
25. Kang, K.M.; Choi, J.U. Growth characteristic of SnO<sub>2</sub> thin film for gas sensor with annealing treatment, *J. Kor. Inst. Surf. Eng.* **2007**, *6*, 258–261.
26. Patel, S.L.; Chander, S.; Purohit, A.; Kannan, M.D.; Dhaka, M.S. Influence of NH<sub>4</sub>Cl treatment on physical properties of CdTe thin films for absorber layer applications. *J. Phys. Chem. Solids* **2018**, *123*, 216–222.
27. Abdulgafour, H.I.; Yusof, Y.; Yam, F.K.; Hassan, Z. Growth of ZnO nanostructures at different temperatures without catalyst by wet thermal oxidation process. *Adv. Mater. Res.* **2013**, *620*, 132–136.
28. Lu, S.; Zhang, Y.; Liu, J.; Li, H.Y.; Hu, Z.; Luo, X.; Gao, N.; Zhang, B.; Jiang, J.; Zhong, A.; et al. Sensitive H<sub>2</sub> gas sensors based on SnO<sub>2</sub> nanowires. *Sens. Actuators B Chem.* **2021**, *345*, 130334.